Modeling strain localisation in a segmented bar by a C^2-continuous two-node integrated-RBF element formulation

D.-A. An-Vo, N. Mai-Duy, C.-D. Tran & T. Tran-Cong
Computational Engineering & Science Research Centre, University of Southern Queensland, Australia

Abstract

We propose a local C^2-continuous 2-node integrated-RBF element (IRBFE) method for the numerical modeling of strain localisation due to material discontinuity in a segmented elastic bar. The proposed local 2-node IRBFE method can be based on structured or unstructured point collocation procedures where both accuracy and efficiency are achieved. We introduce an effective way to exactly handle the material discontinuity by means of integration constants. Numerical results obtained for a bimaterial bar are compared with those from the analytic and finite element methods, demonstrating the advantage of the present approach. It will be shown that the solution is C^2-continuous except at the bimaterial interface where the actual physical discontinuity is captured.
Keywords: integrated-radial-basis-function elements, meshless method, local approximation, segmented bar.

1 Introduction

Recently, considerable research effort in computational mechanics has been devoted to the development of meshless methods such as the element-free Galerkin [1], hp-clouds [2], the reproducing kernel particle [3], the smoothed particle hydrodynamics [4], the diffuse element [5], the partition of unity finite element [6], the natural element [7], meshless Galerkin using radial basis functions [8], the meshless local Petrov-Galerkin (MLPG) [9], the modified smoothed particle hydrodynamics (MSPH) [10], and the collocation method using radial basis functions (RBF) [11]. Among these methods, the MLPG and the RBF collocation

WIT Transactions on Modelling and Simulation, Vol 53,
www.witpress.com, ISSN 1743-3533 (on-line)
doi:10.2495/BE120011

are truly meshless methods. The main objective of the meshless methods is to overcome, or at least alleviate the difficulty of meshing and remeshing the entire structure by adding or discarding nodes at desired location instead. Meshless methods may also alleviate some other problems associated with the finite element method (FEM), such as locking and element distortion. In some meshless methods such as MLPG and global RBF collocation, approximate solutions are continuous for both displacement and strain fields. It is hence widely accepted that, for the analysis of homogeneous problems, meshless methods are more accurate than the finite element method (FEM).

However, practical problems are heterogeneous problems. Examples include structures composing of different components associated with different materials, and composite structures. In the analysis of such problems, the derivative of displacements in direction normal to the interface between two materials must be discontinuous in order for surface tractions there to be continuous. For the analysis of the linear elastostatic problems by the EFG method, Cordes and Moran [12] used the method of Lagrange multipliers, Krongauz and Belytschko [13] employed a special jump function at the line or the surface of discontinuity, and Masuda and Noguchi [14] modified the moving least square (MLS) basis functions so that their derivative jumps at desired locations. Whereas a two-dimensional (2-D) static problem was analyzed by Krongauz and Belytschko [13], a 1-D static problem was scrutinised by Cordes and Moran [12].

Radial basis functions (RBFs) have recently emerged as an attractive tool for the solution of ordinary and partial differential equations (ODEs and PDEs), e.g. [15, 16]. RBF-based approximants can be constructed through a conventional differentiation process, e.g. [11], or an integration process, e.g. [17]. The latter helps avoid the reduction of convergence rate caused by differentiation and provide effective ways of imposing the derivative boundary values. RBF-based approximants can be global or local. Global RBF-based methods are very accurate, e.g. [18, 19]. However, they result in a system matrix that is dense and usually highly ill-conditioned for large problems. The use of RBF-approximants in local forms can help circumvent these difficulties, e.g. [20, 21]. Recently, a local high order approximant based on 2-node elements and integrated RBFs (IRBFs) has been proposed by An-Vo *et al.* [22, 23]. In the proposed 2-node IRBF elements (IRBFEs), the integration constants are exploited to include the first derivatives at the element extremes in the approximations. It was shown that such elements lead to a C^2-continuous solution rather than the usual C^0-continuous solution.

In this paper, we exploit the advantage features of 2-node IRBFE collocation formulation to account for material discontinuities in the analysis of a segmented bar. A novel and accurate treatment for modeling material discontinuity is proposed. The remainder of the paper is organised as follows. Section 2 presents a model of a segmented bar. A brief description of 2-node IRBFEs is given in Section 3 and the proposed method is presented in Section 4. Numerical results are given in Section 5. Section 6 concludes the paper.

2 Model of a segmented bar

Consider a clamped-free bimaterial bar with length L as shown in Figure 1. The material property is discontinuous at $x = d$ where elastic modulus $E(x) = E_1$, $x \in [0, d)$; and $E(x) = E_2$, $x \in (d, L]$. If the bar is subjected to a uniformly distributed axial load P/L, the governing equations can be derived as

$$\frac{\mathrm{d}}{\mathrm{d}x}\left(E_1\frac{\mathrm{d}u}{\mathrm{d}x}\right) + \frac{P}{L} = E_1\frac{\mathrm{d}^2u}{\mathrm{d}x^2} + \frac{P}{L} = 0, \quad x \in [0, d); \tag{1}$$

$$\frac{\mathrm{d}}{\mathrm{d}x}\left(E_2\frac{\mathrm{d}u}{\mathrm{d}x}\right) + \frac{P}{L} = E_2\frac{\mathrm{d}^2u}{\mathrm{d}x^2} + \frac{P}{L} = 0, \quad x \in (d, L]. \tag{2}$$

The exact solution can be verified to be

$$u(x) = \begin{cases} \frac{Px}{E_1}\left(1 - \frac{x}{2L}\right), & x \in [0, d); \\ \frac{Px}{E_2}\left(1 - \frac{x}{2L}\right) + Pd\left(1 - \frac{d}{2L}\right)\left(\frac{1}{E_1} - \frac{1}{E_2}\right), & x \in (d, L]. \end{cases} \tag{3}$$

It can be seen that the derivative of the displacement is discontinuous at $x = d$ where conventional meshless methods fail to capture this discontinuity. In this paper, we propose to use 2-node IRBFEs to approximate the second derivative in (1) and (2). In addition, a novel technique based on 2-node IRBFEs for treating the material discontinuity is proposed.

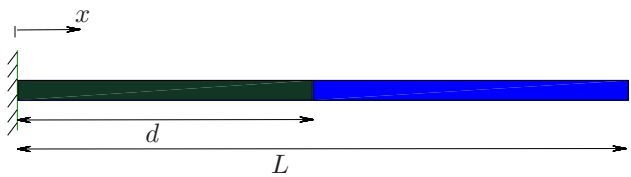

Figure 1: Schematic outline of the problem studied.

3 Two-node IRBFEs

The 1-D problem domain is discretised by a set of uniformly or non-uniformly distributed nodes where pairs of two adjacent nodes form a set of non-overlapping 2-node elements. There are two types of elements, namely interior and semi-interior IRBFEs. An interior element is formed using two adjacent interior nodes while a semi-interior element is generated by an interior node and a boundary node.

3.1 Interior elements

Consider an interior element, $x \in [x_1, x_2]$, and its two nodes are locally named as 1 and 2. Let $\phi(x)$ be a function and ϕ_1, $\mathrm{d}\phi_1/\mathrm{d}x$, ϕ_2 and $\mathrm{d}\phi_2/\mathrm{d}x$ be the values of ϕ

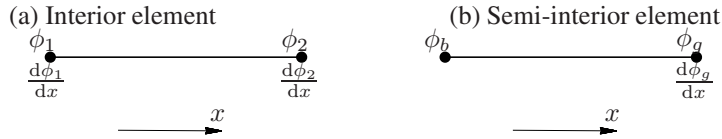

Figure 2: Schematic outline for 2-node IRBFEs.

and $\mathrm{d}\phi/\mathrm{d}x$ at the two nodes, respectively (Figure 2a). The 2-node IRBFE scheme approximates the second-order derivative of $\phi(x)$ using two multiquadric (MQ) functions whose centres are located at x_1 and x_2

$$\begin{aligned}\frac{\mathrm{d}^2\phi}{\mathrm{d}x^2}(x) &= w_1\sqrt{(x-x_1)^2+a_1^2}+w_2\sqrt{(x-x_2)^2+a_2^2}\\ &= w_1 I_1^{(2)}(x)+w_2 I_2^{(2)}(x),\end{aligned} \tag{4}$$

where $I_i^{(2)}(x)$ conveniently denotes the MQ, w_i and a_i are the associated weight and MQ-width at node i ($i = \{1,2\}$). We simply take $a_i = \beta h$, where h is a grid size and β is a factor. First-order derivative of ϕ and the function ϕ are approximated by integrating (4) with respect to x

$$\frac{\mathrm{d}\phi}{\mathrm{d}x}(x) = w_1 I_1^{(1)}(x)+w_2 I_2^{(1)}(x)+C_1, \tag{5}$$

$$\phi(x) = w_1 I_1^{(0)}(x)+w_2 I_2^{(0)}(x)+C_1 x+C_2, \tag{6}$$

where $I_i^{(1)}(x) = \int I_i^{(2)}(x)dx$, $I_i^{(0)}(x) = \int I_i^{(1)}(x)dx$, and C_1 and C_2 are the constants of integration. By collocating (6) and (5) at x_1 and x_2, the relation between the physical space and the RBF coefficient space is obtained

$$\underbrace{\begin{pmatrix}\phi_1\\ \phi_2\\ \frac{\mathrm{d}\phi_1}{\mathrm{d}x}\\ \frac{\mathrm{d}\phi_2}{\mathrm{d}x}\end{pmatrix}}_{\widehat{\phi}} = \underbrace{\begin{pmatrix} I_1^{(0)}(x_1) & I_2^{(0)}(x_1) & x_1 & 1\\ I_1^{(0)}(x_2) & I_2^{(0)}(x_2) & x_2 & 1\\ I_1^{(1)}(x_1) & I_2^{(1)}(x_1) & 1 & 0\\ I_1^{(1)}(x_2) & I_2^{(1)}(x_2) & 1 & 0\end{pmatrix}}_{\mathcal{I}} \underbrace{\begin{pmatrix}w_1\\ w_2\\ C_1\\ C_2\end{pmatrix}}_{\widehat{w}}, \tag{7}$$

where $\widehat{\phi}$ is the nodal-value vector, $\mathcal{I}$ the conversion matrix, and $\widehat{w}$ the coefficient vector. It is noted that not only the nodal values of ϕ but also of $\mathrm{d}\phi/\mathrm{d}x$ are incorporated into the conversion system and this imposition is done in an exact manner owing to the presence of integration constants. Solving (7) yields

$$\widehat{w} = \mathcal{I}^{-1}\widehat{\phi}. \tag{8}$$

Substitution of (8) into (6), (5) and (4) leads to

$$\phi(x) = \left[I_1^{(0)}(x), I_2^{(0)}(x), x, 1\right] \mathcal{I}^{-1}\widehat{\phi}, \tag{9}$$

$$\frac{\mathrm{d}\phi}{\mathrm{d}x}(x) = \left[I_1^{(1)}(x), I_2^{(1)}(x), 1, 0\right] \mathcal{I}^{-1}\widehat{\phi}, \tag{10}$$

$$\frac{\mathrm{d}^2\phi}{\mathrm{d}x^2}(x) = \left[I_1^{(2)}(x), I_2^{(2)}(x), 0, 0\right] \mathcal{I}^{-1}\widehat{\phi}. \tag{11}$$

They can be rewritten in the form

$$\phi(x) = \varphi_1(x)\phi_1 + \varphi_2(x)\phi_2 + \varphi_3(x)\frac{\mathrm{d}\phi_1}{\partial x} + \varphi_4(x)\frac{\mathrm{d}\phi_2}{\partial x}, \tag{12}$$

$$\frac{\mathrm{d}\phi}{\mathrm{d}x}(x) = \frac{\mathrm{d}\varphi_1(x)}{\mathrm{d}x}\phi_1 + \frac{\mathrm{d}\varphi_2(x)}{\mathrm{d}x}\phi_2 + \frac{\mathrm{d}\varphi_3(x)}{\mathrm{d}x}\frac{\mathrm{d}\phi_1}{\mathrm{d}x} + \frac{\mathrm{d}\varphi_4(x)}{\mathrm{d}x}\frac{\mathrm{d}\phi_2}{\mathrm{d}x}, \tag{13}$$

$$\frac{\mathrm{d}^2\phi}{\mathrm{d}x^2}(x) = \frac{\mathrm{d}^2\varphi_1(x)}{\mathrm{d}x^2}\phi_1 + \frac{\mathrm{d}^2\varphi_2(x)}{\mathrm{d}x^2}\phi_2 + \frac{\mathrm{d}^2\varphi_3(x)}{\mathrm{d}x^2}\frac{\mathrm{d}\phi_1}{\mathrm{d}x} + \frac{\mathrm{d}^2\varphi_4(x)}{\mathrm{d}x^2}\frac{\mathrm{d}\phi_2}{\mathrm{d}x}, \tag{14}$$

where $\{\varphi_i(x)\}_{i=1}^4$ is the set of basis functions in the physical space. These expressions allow one to compute the values of ϕ, $\mathrm{d}\phi/\mathrm{d}x$, and $\mathrm{d}^2\phi/\mathrm{d}x^2$ at any point x in $[x_1, x_2]$ in terms of four nodal unknowns, i.e. the values of the field variable and its first-order derivatives at the two extremes (also grid points) of the element.

For convenience, we denote

$$\mu_i = \frac{\mathrm{d}^2\varphi_i(x_1)}{\mathrm{d}x^2}, \tag{15}$$

$$\nu_i = \frac{\mathrm{d}^2\varphi_i(x_2)}{\mathrm{d}x^2}, \quad i = \{1, 2, 3, 4\}. \tag{16}$$

3.2 Semi-interior elements

As mentioned earlier, a semi-interior element is defined by two nodes: an interior node and a boundary node. The subscripts 1 and 2 are now replaced with b (b represents a boundary node) and g (g an interior grid node), respectively (Figure 2b). Assume that the value of ϕ is given at x_b. The conversion system can be formed as

$$\begin{pmatrix} \phi_b \\ \phi_g \\ \frac{\mathrm{d}\phi_g}{\mathrm{d}x} \end{pmatrix} = \begin{pmatrix} I_b^{(0)}(x_b) & I_g^{(0)}(x_b) & x_b & 1 \\ I_b^{(0)}(x_g) & I_g^{(0)}(x_g) & x_g & 1 \\ I_b^{(1)}(x_g) & I_g^{(1)}(x_g) & 1 & 0 \end{pmatrix} \begin{pmatrix} w_b \\ w_g \\ C_1 \\ C_2 \end{pmatrix}. \tag{17}$$

(17) leads to

$$\phi(x) = \varphi_1(x)\phi_b + \varphi_2(x)\phi_g + \varphi_3(x)\frac{\mathrm{d}\phi_g}{\mathrm{d}x}, \tag{18}$$

$$\frac{\mathrm{d}\phi}{\mathrm{d}x}(x) = \frac{\mathrm{d}\varphi_1(x)}{\mathrm{d}x}\phi_b + \frac{\mathrm{d}\varphi_2(x)}{\mathrm{d}x}\phi_g + \frac{\mathrm{d}\varphi_3(x)}{\mathrm{d}x}\frac{\mathrm{d}\phi_g}{\mathrm{d}x}, \tag{19}$$

$$\frac{\mathrm{d}^2\phi}{\mathrm{d}x^2}(x) = \frac{\mathrm{d}^2\varphi_1(x)}{\mathrm{d}x^2}\phi_b + \frac{\mathrm{d}^2\varphi_2(x)}{\mathrm{d}x^2}\phi_g + \frac{\mathrm{d}^2\varphi_3(x)}{\mathrm{d}x^2}\frac{\mathrm{d}\phi_g}{\mathrm{d}x}. \tag{20}$$

For convenience, we denote

$$\theta_i = \frac{\mathrm{d}\varphi_i(x_b)}{\mathrm{d}x}, \quad i = \{1, 2, 3\}. \tag{21}$$

It can be seen that the conversion matrix in (17) is under-determined and its inverse can be obtained using the SVD technique (pseudo-inversion). Owing to the facts that point collocation is used and the RBF conversion matrix is not over-determined, the boundary condition ϕ_b is imposed in an exact manner. For other types of semi-interior elements, the reader is referred to An-Vo *et al.* [22] for details.

4 Proposed 2-node IRBFE collocation method for structures with material discontinuity

4.1 IRBFE collocation method for continuous property regions

Consider node P in Figure 3a where material property is continuous. We can form 2 IRBFEs at P, namely elements MP and PN assumed as interior elements. Both MP and PN can be used to approximate the second-order derivative in equations (1) or (2) at P. We choose MP here and use (14), noting (16), yielding

$$\frac{\mathrm{d}^2 u_P}{\mathrm{d}x^2} = \nu_1 u_M + \nu_2 u_P + \nu_3 \frac{\mathrm{d}u_M}{\mathrm{d}x} + \nu_4 \frac{\mathrm{d}u_P}{\mathrm{d}x}. \tag{22}$$

It can be seen that there are two unknowns at P, i.e. u_P and $\mathrm{d}u_P/\mathrm{d}x$. One thus needs to generate two independent equations. The first equation is obtained by conducting point collocation of the governing equation at P, i.e. by substituting (22) into (1) or (2). The other equation can be formed by enforcing the local continuity of $\mathrm{d}^2u/\mathrm{d}x^2$ across the elements at P

$$\left(\frac{\mathrm{d}^2 u_P}{\mathrm{d}x^2}\right)_L = \left(\frac{\mathrm{d}^2 u_P}{\mathrm{d}x^2}\right)_R, \tag{23}$$

where $(.)_L$ indicates that the computation of $(.)$ is based on the element to the left of P, i.e. element *MP*, and similarly subscript *R* denotes the right element *PN*. The left of equation (23) is replaced by (22) and the right by a similar expression

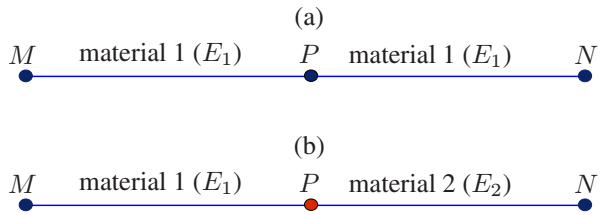

Figure 3: Material property at a nodal point P can be continuous (a) and discontinuous (b).

obtained via (14), noting (15), yielding

$$\nu_1 u_M + \nu_2 u_P + \nu_3 \frac{\mathrm{d}u_M}{\mathrm{d}x} + \nu_4 \frac{\mathrm{d}u_P}{\mathrm{d}x} = \mu_1 u_P + \mu_2 u_N + \mu_3 \frac{\mathrm{d}u_P}{\mathrm{d}x} + \mu_4 \frac{\mathrm{d}u_N}{\mathrm{d}x}. \quad (24)$$

4.2 Proposed treatment for material property discontinuity

If the material property is discontinuous at P as shown in Figure 3b, elastic moduli E_1 and E_2 are associated with regions to the left and right of P respectively. At P, the displacement field is continuous and the strain field is discontinuous. As a result, we have a unique value of displacement u_P and two different values of strain, namely $(\mathrm{d}u_P/\mathrm{d}x)_L$ and $(\mathrm{d}u_P/\mathrm{d}x)_R$, to the left and right side of P respectively. The continuous condition of stress field at P yields

$$E_1 \left(\frac{\mathrm{d}u_P}{\mathrm{d}x} \right)_L = E_2 \left(\frac{\mathrm{d}u_P}{\mathrm{d}x} \right)_R. \quad (25)$$

We propose to approximate the left and the right of (25) by elements MP and PN, respectively, as semi-interior elements here. Consider that $M \equiv g$, $P \equiv b$ in the former; $P \equiv b$, $N \equiv g$ in the latter and make use of (19), noting (21), equation (25) becomes

$$E_1 \left(\theta_1 u_P + \theta_2 u_M + \theta_3 \frac{\mathrm{d}u_M}{\mathrm{d}x} \right) = E_2 \left(\theta_1 u_P + \theta_2 u_N + \theta_3 \frac{\mathrm{d}u_N}{\mathrm{d}x} \right). \quad (26)$$

It is noted that (22) and (24) will be slightly different if M or N is at the Dirichlet boundary or at the bimaterial interface where (20) for semi-interior elements is used instead of (14).

Collection of the discretised equations (22), continuity equations (24) at the appropriate nodal points P, and (26) at the bimaterial interface leads to a square system of algebraic equations that is very sparse and banded. This system of equations is solved to yield for the displacement field at all nodal points and the strain field at all nodal points except the nodal point at the bimaterial interface. It can be seen that the solution is C^2-continuous except at the bimaterial interface which is what it should be.

5 Numerical results

The proposed method denoted by IRBFE-WT is applied to solve a simple clamped-free bimaterial bar governed by equations (1) and (2). Material parameters are $E_1 = 200\,\text{GPa}$, $E_2 = 70\,\text{GPa}$. The geometry is defined by $L = 50\,\text{mm}$, $d = L/2 = 25\,\text{mm}$. The numerical value of P has been chosen as $P = -100\,\text{MPa}$. The results are compared with an IRBFE collocation method without the discontinuity treatment (denoted by IRBFE-WoT), FEM, and the analytic solution given in (3).

Figure 4 displays the axial displacement and strain along the bar by using 21 uniformly distributed nodes and $\beta = 15$. IRBFE-WoT method cannot capture the exact displacement and strain fields while results by using IRBFE-WT method are in good agreement with the exact solution. FEM gives a zigzag strain field as shown in Figure 4b.

Table 1 presents errors obtained by the present method, the IRBFE-WoT and FEM using 11 uniformly distributed nodes. IRBFE-WT and IRBFE-WoT are conducted in a wide range of MQ-width parameter β. It can be seen that by increasing the value of β the accuracy is improved significantly by the IRBFE-WT

Table 1: Relative L_2 errors of the axial displacement u and the axial strain $\mathrm{d}u/\mathrm{d}x$ by using 11 uniformly distributed nodes and increasing values of β. Note that $a(b)$ means $a \times 10^b$, IRBF1=IRBFE-WoT, and IRBF2=IRBFE-WT.

	$Ne(u)$			$Ne(\mathrm{d}u/\mathrm{d}x)$		
β	IRBF1	IRBF2	FEM	IRBF1	IRBF2	FEM
1	6.27(-1)	5.09(-2)	4.10(-3)	7.61(-1)	1.02(-1)	7.82(-2)
5	7.04(-1)	3.20(-3)		8.31(-1)	6.50(-3)	
10	7.08(-1)	8.28(-4)		8.35(-1)	1.70(-3)	
15	7.09(-1)	3.69(-4)		8.35(-1)	7.39(-4)	
20	7.09(-1)	2.09(-4)		8.36(-1)	4.16(-4)	
30	7.09(-1)	9.25(-5)		8.36(-1)	1.85(-4)	
40	7.09(-1)	5.21(-5)		8.36(-1)	1.04(-4)	
50	7.09(-1)	3.33(-5)		8.36(-1)	6.66(-5)	
60	7.09(-1)	2.31(-5)		8.36(-1)	4.63(-5)	
70	7.09(-1)	1.70(-5)		8.36(-1)	3.40(-5)	
100	7.09(-1)	8.33(-6)		8.36(-1)	1.67(-5)	

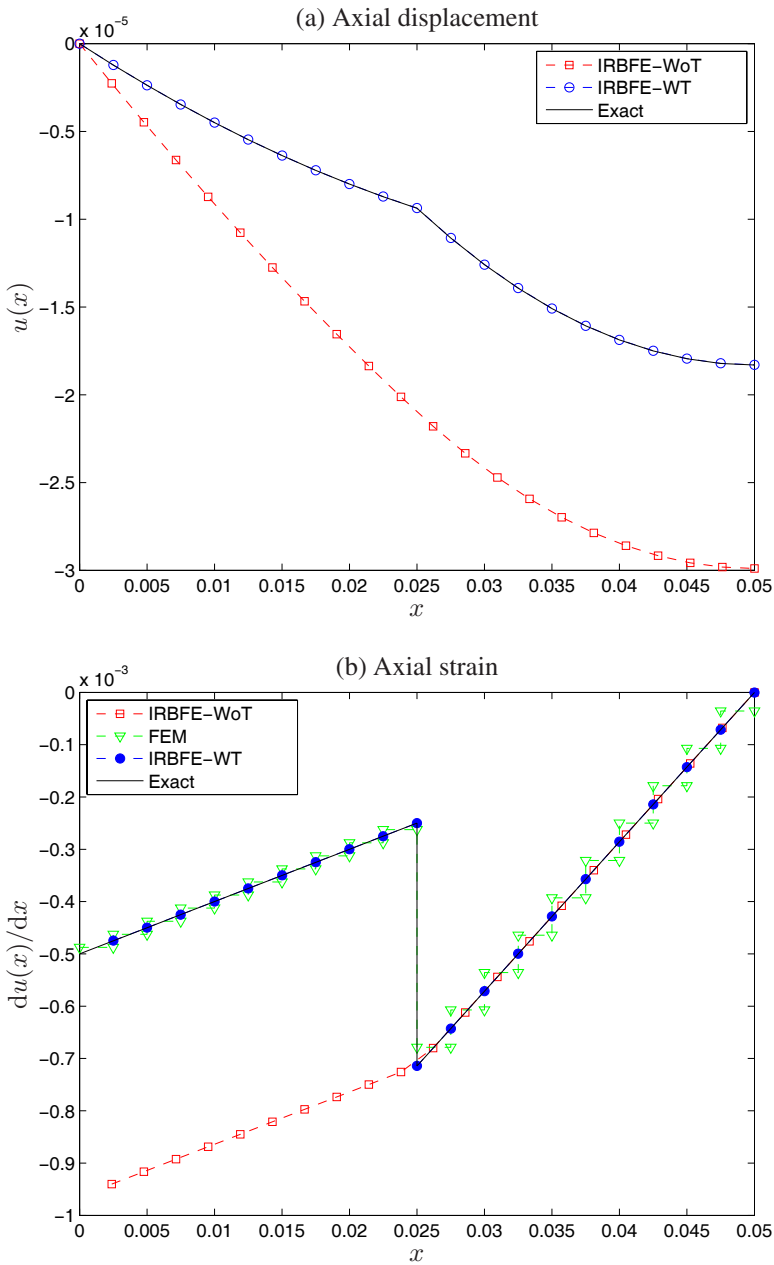

Figure 4: Axial displacement and strain by using 21 uniformly distributed nodes and $\beta = 15$.

method. At $\beta = 100$, IRBFE-WT gives about 3 orders of magnitude improvement for both displacement and strain fields in comparison with FEM.

6 Concluding remarks

In this paper, we have successfully developed a high-order collocation method based on 2-node IRBFEs for structures with material interface. The proposed method can capture the discontinuity of the strain field accurately.

Acknowledgements

D.-A. An-Vo would like to thank USQ, FoES and CESRC for a PhD scholarship. This work was supported by the Australian Research Council.

References

[1] T. Belytschko, Y. Y. Lu, and L. Gu. Element-free Galerkin methods. *International Journal for Numerical Methods in Engineering*, 37:229–256, 1994.

[2] C.A.M Duarte and J.T. Oden. Hp clouds-an hp meshless method. *Numerical Methods for Partial Differential Equations*, 12:673–705, 1996.

[3] W. K. Liu, S. Jun, J. Adee, and T. Belytschko. Reproducing kernel particle methods for structural dynamics. *International Journal for Numerical Methods in Engineering*, 38:1655–1679, 1995.

[4] L. B. Lucy. A numerical approach to the testing of the fission hypothesis. *The Astronomical Journal*, 82:1013–1024, 1977.

[5] B. Nayroles, G. Touzot, and P. Villon. Generalizing the finite element method: diffuse approximation and diffuse elements. *Computational Mechanics*, 10:307–318, 1992.

[6] J. M. Melenk and I. Babuska. The partition of unity finite element method: basis theory and applications. *Computer Methods in Applied Mechanics and Engineering*, 139:289–314, 1996.

[7] N. Sukumar, B. Moran, and T. Belytschko. The natural element method in solid mechanics. *International Journal for Numerical Method in Engineering*, 43:839–887, 1998.

[8] H. Wendland. Piecewise polynomial, positive definite and compactly supported radial basis functions of minimal degree. *Advances in Computational Mathematics*, 4:389–396, 1995.

[9] S. N. Atluri and S. P. Shen. The meshless local Petrov-Galerkin (MLPG) approach in computational mechanics. *Computational Mechanics*, 22:2117–2127, 1998.

[10] G. M. Zhang and R. C. Batra. Modified smoothed particle hydrodynamics method and its application to transient problems. *Computational Mechanics*, 34:137–146, 2004.

[11] E.J. Kansa. Multiquadrics-a scattered data approximation scheme with applications to computational fluid-dynamics-II: Solution to parabolic, hyperbolic and elliptic partial differential equations. *Computers & Mathematics with Applications*, 19:147–161, 1990.
[12] L. W. Cordes and B. Moran. Treatment of material discontinuity in the element-free Galerkin method. *Computer Methods in Applied Mechanics and Engineering*, 139:75–89, 1996.
[13] Y. Krongauz and T. Belytschko. EFG approximation with discontinuous derivatives. *International Journal for Numerical Method in Engineering*, 41:1215–1233, 1998.
[14] S. Masuda and H. Noguchi. Analysis of structure with material interface by meshless method. *CMES: Computer Modeling in Engineering and Sciences*, 11(3):131–143, 2006.
[15] G. E. Fasshauer. *Meshfree approximation methods with Matlab*. Interdisciplinary mathematical sciences, vol. 6. Singapore: World Scientific Publishers, 2007.
[16] S. N. Atluri and S. Shen. *The meshless local Petrov-Galerkin (MLPG) method*. Tech Science Press, 2002.
[17] N. Mai-Duy and T. Tran-Cong. Numerical solution of differential equations using multiquadric radial basis function networks. *Neural Networks*, vol. 14:185–199, 2001.
[18] A. H. D. Cheng, M. A. Golberg, E. J. Kansa, and G. Zammito. Exponential convergence and h-c multiquadric collocation method for partial differential equations. *Numerical Methods for Partial Differential Equations*, 19:571–594, 2003.
[19] C.-S. Huang, C.-F. Lee, and A.H.-D. Cheng. Error estimate, optimal shape factor, and high precision computation of multiquadric collocation method. *Engineering Analysis with Boundary Elements*, 31:614–623, 2007.
[20] C. Shu, H. Ding, and K.S. Yeo. Local radial basis function-based differential quadrature method and its application to solve two-dimensional incompressible Navier-Stokes equations. *Computer Methods in Applied Mechanics & Engineering*, vol. 192:941–954, 2003.
[21] E. Divo and A.J. Kassab. An efficient localized radial basis function meshless method for fluid flow and conjugate heat transfer. *Journal of Heat Transfer*, vol. 129:124–136, 2007.
[22] D.-A. An-Vo, N. Mai-Duy, and T. Tran-Cong. A C^2-continuous control-volume technique based on Cartesian grids and two-node integrated-RBF elements for second-order elliptic problems. *CMES: Computer Modeling in Engineering and Sciences*, 72 (4):299–334, 2011.
[23] D.-A. An-Vo, N. Mai-Duy, and T. Tran-Cong. High-order upwind methods based on C^2-continuous two-node integrated elements for viscous flows. *CMES: Computer Modeling in Engineering and Sciences*, 80 (2):141–177, 2011.